Normal metal tunnel junction-based superconducting quantum interference proximity transistor: the N-SQUIPT

Sophie D'Ambrosio, ^{1, a)} Martin Meissner, ¹ Christophe Blanc, ¹ Alberto Ronzani, ¹ and Francesco Giazotto ^{1, b)} *NEST Istituto Nanoscienze-CNR and Scuola Normale Superiore, I-56127 Pisa, Italy*

We report the fabrication and characterization of an alternative design for a superconducting quantum interference proximity transistor (SQUIPT) based on a normal metal (N) probe. The absence of direct Josephson coupling between the proximized metal nanowire and the N probe allows us to observe the full modulation of the wire density of states around zero voltage and current *via* the application of an external magnetic field. This results into a drastic suppression of power dissipation which can be as low as a few $\sim 10^{-17}$ W. In this context the interferometer allows an improvement of up to four orders of magnitude with respect to earlier SQUIPT designs, and makes it ideal for extra-low power cryogenic applications. In addition, the N-SQUIPT has been recently predicted to be the enabling candidate for the implementation of coherent caloritronic devices based on proximity effect.

The superconducting quantum interference proximity transistor (SQUIPT) is a magnetic-flux detector alternative to the widespread superconducting quantum interference device (SQUID)¹. Based on the proximity effect^{2–7}, it is considered a promising candidate for several advanced applications such as the next generation of ultra-high sensitive and ultra-low power magnetometers^{8–11}. The SQUIPT is a two-terminal device made of a normal metal (N) nanowire embedded into a superconducting (S) ring, and coupled via a tunnel barrier to a probing electrode (see Fig. 1). The N nanowire, in clean metallic contact with the S ring, is proximized by the latter, and forms a SNS Josephson weak link. In this configuration, the density of states (DOS) of the N wire is modulated by the application of an external magnetic flux Φ piercing the loop, and enables the transition of the wire from the N- to the S-like state 13-23.

Since its original introduction, the SQUIPT has been exclusively implemented with a tunnel superconducting probe (S-SQUIPT) because of its sharper response and improved noise performance^{1,8–12}. Yet, it has been recently predicted that coherent thermal valves based on the proximity effect privilege SQUIPTs realized with a normal metal probe (N-SQUIPT), as the presence of the superconducting junction in the conventional S-SOUIPT design would severely limit the heat flow across the structure²⁴. The N-SQUIPT appears therefore as a highly-promising candidate to implement future phasecoherent caloritronic devices such as heat transistors, rectifiers, thermal splitters and phase-tunable electron coolers²⁵. Besides the foreseen advantages in coherent caloritronics, the N-SOUIPT shows attractive performance for more conventional electronic applications due to the lack of Josephson coupling. The N probe offers the possibility to operate the device around zero bias therefore allowing to reach extra-low power dissipation, down to a few tens of aW, which lowers by up to four orders of magnitude the previous achieved dissipation values 9-11.

Here we report the fabrication and the magneto-electric characterization of Al/Cu-based N-SQUIPTs. After describing the different steps required to realize this device, we will

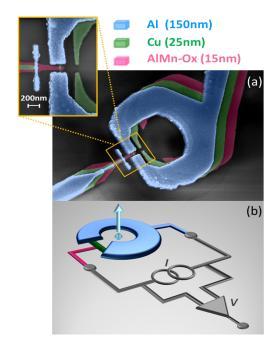


FIG. 1. (Color online) (a) Pseudo-color tilted scanning electron micrograph (SEM) of a typical N-SQUIPT. The Cu normal metal wire is in clean metallic contact with the Al superconductive ring. An $Al_{0.98}Mn_{0.02}$ normal metal tunnel probe is connected to the middle of the Cu nanowire. The zoomed image on the left inset emphasises the core of the device close to the SNS weak link. (b) Sketch of N-SQUIPT current bias measurement setup under fixed current-bias (1). Φ symbolizes the externally applied magnetic flux piercing the loop whereas V is the voltage drop.

show the full electric behavior as a function of bath temperature. Our results are reproduced with the Usadel equations describing the proximity effect in the N wire. Moreover, the N-SQUIPTs are characterized by a maximum flux-to-voltage transfer function of ~ 0.45 mV/ Φ_0 and maximum flux-to-current transfer function of ~ 12 nA/ Φ_0 .

Figure 1 (a) shows a scanning electron microscopy (SEM) image of a typical N-SQUIPT device. The samples have been fabricated through electron-beam lithography (EBL) and three-angle shadow-mask evaporation performed on an oxidized Si wafer covered with a suspended bilayer resist mask made of 900-nm-thick copolymer layer and 300-nm-thick

a) Electronic mail: sophie.dambrosio@nano.cnr.it

b) Electronic mail: francesco.giazotto@sns.it

	l	d	w	R_T	$ dI/d\Phi _{Max}$	$ dV/d\Phi _{Max}$
Sample	(nm)	(nm)	(nm)	$(k\Omega)$	(nA/Φ_0)	(mV/Φ_0)
A	160	60	120	33	12	0.45
В	160	55	120	36	11.5	0.41
C	150	60	90	40	12	0.46

TABLE I. Parameters of three different N-SQUIPT samples measured at $T_{bath} = 25$ mK. The symbols l and d are used to denote the length and the width of the N nanowire, respectively, whereas w indicates the width of N probe. R_T is the normal-state tunnel junction resistance of the N probe. $|dI/d\Phi|_{\text{Max}}$ and $|dV/d\Phi|_{\text{Max}}$ are the maximum absolute value of the flux-to-current and flux-to-voltage transfer functions, respectively.

polymethyl methacrylate (PMMA) layer spun on top of it. The EBL step is followed by development in methyl isobutyl ketone:isopropanol (MIBK:IPA) 1:3 solution for 1 min, rinsing in IPA and then drying. The different metal layers are deposited by ultra-high vacuum electron-beam evaporation at different angles. At first 15 nm of Al_{0.98}Mn_{0.02} are deposited at 40° and oxidized for 5 min with an oxygen pressure of 37 mTorr to realize the probe electrode, then 25 nm of Cu are evaporated at 20° to form the proximized N wire, and finally a 150-nm-thick Al superconductor ring is deposited at zero angle. The oxidation of the N probe is crucial to make functional our device. It insures a well-defined voltage bias allowing the measurement of the DOS, and avoids as well any weakening effect due to the inverse proximity effect. Furthermore concerning the caloritronic applications, the control of the resistivity through the tunnel barrier allows us to limit the power dissipation of our system. To achieve full phase polarizability the SQUIPT requires to have an S ring with a thickness much larger than the wire in order to reach the condition $L^R \ll L^{WL}$, where $L^{R(WL)}$ denotes the inductance of the ring(weak link)^{9–11}. The value of the ring inductance has been estimated with the finite-elements software FastHenry²⁶ to be less than 5 pH.

We have measured our N-SQUIPTs in a He³-He⁴ dilution refrigerator at different temperatures ranging from 25 mK to 1.2 K using room temperature preamplifiers. The main characteristics of our devices, summarized in Tab. I, demonstrate the good level of reproducibility achieved with the fabrication process described. In the following we report the measurements obtained for sample A, the other samples showing similar results. From the length l of the N wire, we deduce the Thouless energy $E_{Th} = \hbar D/l^2 \simeq 0.8 \, \Delta_0$, by using $D \simeq 60 \, \mathrm{cm}^2 \mathrm{s}^{-1}$ for the diffusion coefficient in the Cu wire, and $\Delta_0 \simeq 190 \, \mu \mathrm{eV}$ as the zero-temperature energy gap in the Al loop which are estimated from previous works¹¹. The above given value for the ratio E_{Th}/Δ_0 sets the frame of the *intermediate-length* junction regime of the SNS weak link.

Figures 2(a) and (b) show the current $I(V_{bias})$ and the differential conductance $dI/dV(V_{bias})$ measured for different magnetic flux Φ applied orthogonally to the ring at $T_{bath}=25$ mK [see Fig. 1(b)]. Data show evidence of the full wire DOS modulation, the N wire going from the S-like state with a maximum induced minigap $\Delta_w \simeq 160~\mu eV$ at $\Phi=0$, to the N-like

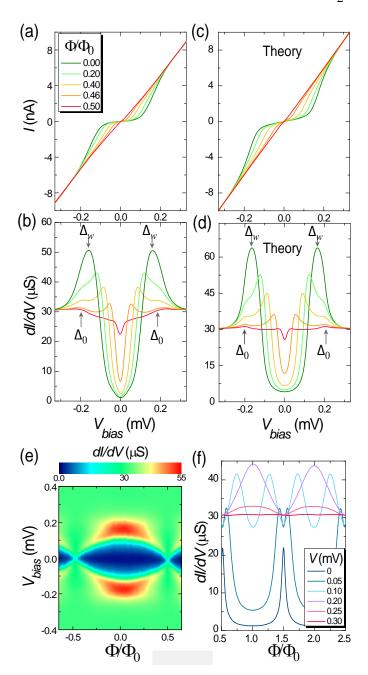


FIG. 2. (Color online) (a) Current versus voltage $I(V_{bias})$ measured at different magnetic flux Φ and T_{bath} =25 mK. (b) Differential conductance versus voltage $dI/dV(V_{bias})$ measured for Φ and T_{bath} as in (a). (c) and (d) Theoretical calculations of the curves shown in panels (a) and (b), respectively. Δ_0 is the zero-temperature energy gap in the Al loop and Δ_w the maximum induced minigap in the Cu nanowire at $\Phi=0$. (e) Color plot of the differential conductance versus voltage and magnetic flux $dI/dV(V_{bias},\Phi)$ measured at T_{bath} =25 mK. (f) Differential conductance versus magnetic flux $dI/dV(\Phi)$ measured at various voltages and T_{bath} =25 mK.

state $\Delta_w \simeq 0$ at $\Phi/\Phi_0 = 0.5$, where $\Phi_0 = 2.067 \times 10^{-15}$ Wb is the flux quantum. From the curves of the differential conductance displayed in Fig. 2(b), we can estimate the Al ring gap

 $\Delta_0 \simeq 190~\mu eV$ which appears as a peak at higher voltage for $\Phi \neq 0$ and the maximum value of the Cu minigap $\Delta_w \simeq 160~\mu eV$ corresponding to the position of the peaks at $\Phi = 0$, as shown by the arrows in Fig. 2(b). Both values are consistent with the prediction obtained from the solution of the quasiclassical equations as explained below.

The overall theoretical comparison to the experimental data of Figs. 2(a) and (b) is presented in Figs. 2(c) and (d), respectively, and demonstrates a fairly good qualitative agreement with the experiment. These calculations have been obtained from the solution of the Usadel equations²⁷ which describes the proximity effect in the diffusive N wire, and can be written as

$$\hbar D \partial_x^2 \gamma_{1,2} - \hbar D \frac{2\gamma_{2,1}}{1 + \gamma_1 \gamma_2} (\partial_x \gamma_{1,2})^2 + 2i(E + i\Gamma)\gamma_{1,2} = 0, \quad (1)$$

where the first equation corresponds to the first index of γ and the second equation to the second index^{28,29}. The functions $\gamma_{1,2}$ determined with Riccati parametrization^{30,31} are used to describe the retarded Green function $\mathcal{G}(x, E, \Phi, T) = (1-\gamma_1\gamma_2)/(1+\gamma_1\gamma_2)$, and are dependent of the position x, the energy E, the flux Φ , and the temperature T as well. The DOSs in the normal proximized region can be expressed by $\mathcal{N}_N(x, E, \Phi, T) = \text{Re}[\mathcal{G}(x, E, \Phi, T)]$. The value $\Gamma = 0.065 \ \Delta_0$ is taken as input parameter, and describes the inelastic scattering present in the N region. Here the Nazarov boundary conditions^{32,33} are used in order to include in the simulation details such as the quality of the normal metal-superconductor interfaces in the SNS weak link³⁴. The current flowing through the N probe can be written as

$$I(\Phi, V, T) = \frac{1}{eR_{TW}} \int_{0}^{w} dx \int_{-\infty}^{\infty} dE \, \mathcal{N}_{N}(x, E, \Phi, T)$$

$$\times \left[\mathcal{F}_{0}(E - eV, T) - \mathcal{F}_{0}(E, T) \right],$$
(2)

where e is the electron charge, \mathcal{F}_0 is the Fermi distribution function and $\mathcal{N}_N(x,E,\Phi,T)$ is calculated by solving Eqs. 1. The I(V) curves shown in Fig. 2(c) directly correspond to the calculation of Eq. 2 with $T_{bath}=25$ mK and Φ values as in Fig. 2(a). The differential conductances traces displayed Fig. 2(d) are the derivatives of the curves shown in Fig. 2(c). From Fig. 2(d), we confirm the value $\Delta_0 \simeq 190$ μeV of the S ring which corresponds to a critical temperature $T_C = \Delta_0/(1.764k_B) \simeq 1.2$ K. We extract as well the effective N wire minigap $\Delta_w \simeq 160~\mu \text{eV}$ at $\Phi=0$.

The color plot of $dI/dV(V_{bias},\Phi)$ shown in Fig. 2(e) gives a direct observation of the DOS modulation which goes from a fully developed minigap at $\Phi=0$, to an almost closed minigap at $|\Phi/\Phi_0|=0.5$ with a behavior which is Φ_0 -periodic in the magnetic flux^{2,35}.

Figure 2(f) shows the differential conductance $dI/dV(\Phi)$ at different values V_{bias} , and provides the experimental evidence that an appreciable magnetic flux response in the differential conductance values is obtained with an extra-low dissipation measurement setup. Indeed, the observed modulations have been measured with a lock-in amplifier with an input amplitude modulation $V_{AC} \simeq 10^{-6}$ V. At V=0 the typical output current level is $I_{AC} \simeq 10^{-11}$ A with an average total power

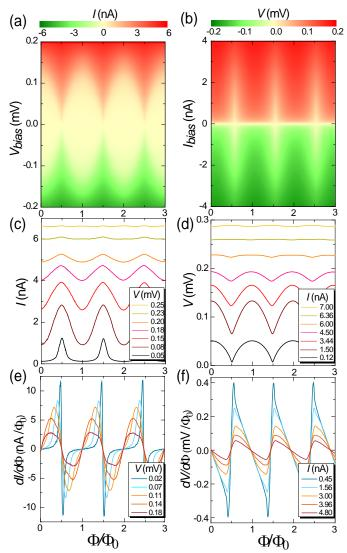


FIG. 3. (Color online) (a) and (b) Color plots which present the flux-modulated current as a function of voltage $I(V_{bias}, \Phi)$ and the flux-modulated voltage as a function of current $V(I_{bias}, \Phi)$ at T_{bath} =25 mK, respectively. (c) Curves of flux-modulated current at different voltage values selected from (a). (d) Curves of flux-modulated voltage at different current values selected from (b). (e) and (f) Flux-to-current $(dI/d\Phi)$, and flux-to-voltage $(dV/d\Phi)$ transfer function curves obtained from the derivative of the $I(\Phi)$ and $V(\Phi)$ measurements, respectively.

dissipation for the N-SQUIPT around 10^{-17} W. The typical value of the dynamic resistance (on the order of 30 k Ω) sets the limit of the reachable bandwidth depending on the shunt capacitance typically due to line filtering³⁶.

Figure 3 completes the electrical characterization of our device. In particular, Figs. 3(a) and (b) show the color plots of $I(V_{bias}, \Phi)$ and $V(I_{bias}, \Phi)$, respectively. Figures 3(c) and (d) display a cross section of the above color plots for some selected values of V_{bias} and I_{bias} . A careful inspection of Figs. 3(a) and (b) indicates that the measured current and voltage modulations reach peak-to-peak amplitudes as large as $\delta I = 2$ nA and $\delta V \simeq 90~\mu V$, respectively. We note that the lower value for δV in comparison to the full minigap ampli-

tude $\Delta_w \simeq 160 \ \mu eV$ can be reproduced in our simulation by including terms related to a finite inelastic scattering in the N wire and to a non ideal Al/Cu interface transmissivity³⁴ [see Figs. 2(c) and (d)].

The SQUIPT behaves as a flux-to-current or a flux-to-voltage transformer whose response efficiency can be quantified by the maximum absolute value of its flux-to-current ($|dI/d\Phi|_{\text{Max}}$) or flux-to-voltage ($|dV/d\Phi|_{\text{Max}}$) transfer functions, respectively ^{1,8–11}. In our case, this information is shown in Figs. 3(e) and (f), respectively. Their values reach $|dV/d\Phi|_{\text{Max}} \simeq 0.45 \text{ mV}/\Phi_0$ and $|dI/d\Phi|_{\text{Max}} \simeq 12 \text{ nA}/\Phi_0$ at 25 mK, respectively (see Tab. I). Although higher values have been reported in S-SQUIPTs ^{10,11}, the N-SQUIPTs still exhibit performance on par with conventional state-of-art SQUID sensors ³⁷.

We now discuss the noise-equivalent-flux (NEF) or flux resolution (Φ_{NS}) of the N-SQUIPT. The intermediate value of the tunnel junction impedance allows the devices to be operated either with voltage amplification under DC current bias or with current amplification under DC voltage bias. In the former configuration a maximum voltage responsivity $|dV/d\Phi|_{\text{Max}} \simeq 0.45 \,\text{mV}/\Phi_0$ has been recorded with $I_{bias} \simeq 400 \, \mathrm{pA}$, corresponding to $\Phi_{NS} = \sqrt{S_V}/\left| dV/d\Phi \right|_{Max} \simeq$ $3.4 \mu \Phi_0 / \sqrt{\text{Hz}}$, where $\sqrt{S_V}$ is the input-referred noise power spectral density of the preamplifier used in this setup³⁸. Improved performance can be obtained by exploiting the low input-referred noise level granted by a transimpedance current preamplifier³⁹ combined with the significant current responsivity $|dI/d\Phi|_{\text{Max}} \simeq 12 \,\text{nA}/\Phi_0$ achieved at $V_{bias} \simeq 20 \,\mu\text{V}$. In this configuration the achievable magnetic flux resolution is expected to be limited by the shot noise of the tunnel junction, reaching values as low as $\Phi_{NS} = \sqrt{2eI}/|dI/d\Phi|_{Max} \simeq$ $1.5 \mu \Phi_0 / \sqrt{\text{Hz}}$, where $I \simeq 1 \text{ nA}$. The magnitude of the dissipation induced in the DC readout is of the order of tens of fW. We notice that the contribution due to the presence of a finite ring inductance in the noise performance is negligible 40.

As already noted, the N-SQUIPT can also be operated at zero DC bias, where its response can be linearized. In this configuration the operating power can be brought down to the aW range by applying a minute AC excitation, with the same technique which is used in resistance bridges adapted to cryogenic thermometry. The maximal zero-bias conductance responsivity estimated from the data shown in Fig. 2(f) is $|dG_0/d\Phi|_{Max} \simeq 450 \,\mu\text{S}/\Phi_0$, leading to a magnetic flux resolution $\Phi_{NS} = \sqrt{S_G}/\left| dG_0/d\Phi \right|_{Max} \simeq 300 \, \mu \Phi_0/\sqrt{Hz}$, where $\sqrt{S_G} \simeq 140\,\mathrm{nS}/\sqrt{\mathrm{Hz}}$ is the noise-equivalent power spectral density of the lock-in amplification setup. This value of the flux resolution has been obtained with a 1- μV AC voltage excitation, corresponding to ~ 17 aW of applied power. The impact of temperature T is displayed in Fig. 4. In particular, Fig. 4(a) shows the evolution of $I(V_{bias})$ at different temperatures when the minigap in the N wire DOS is fully developed (i.e. at $\Phi = 0$). As expected, when T increases, the proximity effect in the SNS junction is progressively weakened and completely disappears at 1.2 K which corresponds to the critical temperature of the Al ring. Figure 4(b) shows the corresponding differential conductance and confirms the suppression of the minigap at T_C . The increase in temperature leads to a re-

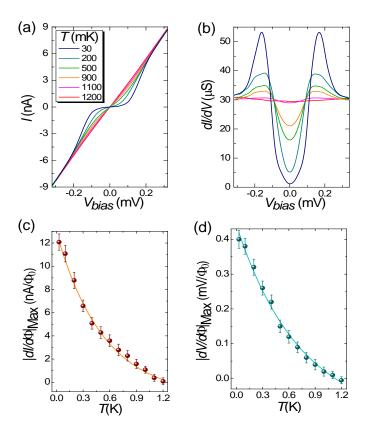


FIG. 4. (Color online) (a) Current versus voltage $I(V_{bias})$ measured for various bath temperatures T_{bath} at $\Phi = 0$. (b) Differential conductance $dI/dV(V_{bias})$ for the same temperatures as in (a). (c) and (d) Temperature dependence of the maximum flux-to-current and flux-to-voltage transfer functions, respectively. The error bars shown in (c) and (d) represent the standard deviation of maximum values estimated from $I(\Phi)$ and $V(\Phi)$ data over several flux periods. The lines connecting the experimental data in (c) and (d) are an interpolation to guide the eye.

duction of $V(\Phi)$ and $I(\Phi)$ which, as a consequence, suppresses the amplitude of the flux-to-voltage and flux-to-current transfer functions, as shown in Figs. 4(c) and (d), respectively. We emphasize that the N-SQUIPT shows appreciable values for both the maximum flux-to-voltage and flux-to-current transfer functions even at somewhat high bath temperatures. In particular, at 1 K our interferometers still exhibit $|dI/d\Phi|_{\rm Max} \simeq 1$ nA/ Φ_0 and $|dV/d\Phi|_{\rm Max} \simeq 30~\mu V/\Phi_0$.

In summary, we have performed the fabrication and the magneto-electrical characterization of Al/Cu-based N-SQUIPTs. The design choice of the N probe characterized by the absence of the Josephson coupling with the proximized weak link shows several advantages: i) the transition between a fully linear to a highly nonlinear characteristic (unlike the S-SQUIPT in which only nonlinear behavior is possible) suggests the adoption of the N-SQUIPT as a fully metallic, highly-efficient, tunable electrical diode for operation at temperature below 1K. ii) The typical operating power, fully modulated from fW to aW levels, gives the opportunity of using the N-SQUIPT as a magnetometer for condensed matter

systems⁴¹ characterized by low-energy excitations, which are vulnerable to disruption by measurement back-action. iii) The choice of a normal metal probe has been shown to improve drastically the transport properties of a heat nanovalve²⁴ due to the lack of a superconducting gap in the probe itself. More generally, a normal density of states provides a natural opportunity of realizing a thermal reservoir in which the electron temperature can be tuned and probed to its fullest extent. These properties make the N-SQUIPT a privileged building block for the implementation of coherent caloritronic devices based on proximity effect.

The authors thanks C. Altimiras, F. S. Bergeret and E. Strambini for fruitful comments. The European Research Council under the European Union's Seventh Framework Program (FP7/2007-2013)/ERC Grant agreement No. 615187-COMANCHE and MIUR-FIRB2013 – Project Coca (Grant No. RBFR1379UX) are acknowledge for partial financial support.

- ¹F. Giazotto, J. T. Peltonen, M. Meschke, and J. P. Pekola, Nat. Phys. **6**, 254 (2010)
- ²P. G. de Gennes, *Superconductivity of Metals and Alloys* (Benjamin, New York, 1966).
- ³P. G de Gennes, Rev. Mod. Phys. **36**, 225 (1964).
- ⁴A. I. Buzdin, Rev. Mod. Phys. **77**, 935 (2005).
- ⁵F. Zhou, P. Charlat, B. Spivak, and B. Pannetier, J. Low Temp. Phys. **110**, 841 (1998).
- ⁶W. Belzig, F. K. Wilhelm, C. Bruder, G. Schön, and A. D. Zaikin, Superlattices Microstruct. 25, 1251 (1999).
- ⁷V. Yu Nazarov, Superlattices Microstruct. **25**, 1221 (1991).
- ⁸F. Giazotto and F. Taddei, Phys. Rev. B **84**, 214502 (2011).
- ⁹M. Meschke, J. T. Peltonen, J. P. Pekola, and F. Giazotto, Phys. Rev. B 84, 214514 (2011).
- ¹⁰R. N. Jabdaraghi, M. Meschke, and J. P. Pekola, Appl. Phys. Lett. **104**, 082601 (2014).
- ¹¹A. Ronzani, C. Altimiras, and F. Giazotto, Phys. Rev. Appl. 2, 024005 (2014).
- ¹²M. Alidoust, K. Halterman, and J. Linder Phys. Rev. B **88**, 075435 (2013).
- ¹³H. le Sueur, P. Joyez, H. Pothier, C. Urbina, and D. Esteve, Phys. Rev. Lett. 100, 197002 (2008).
- ¹⁴B. D. Josephson, Phys. Lett. 1, 251 (1962).
- ¹⁵K. K. Likharev, Rev. Mod. Phys. **51**, 101 (1979).

- ¹⁶R. Doll and M. Näbauer, Phys. Rev. Lett. **7**, 51 (1961).
- ¹⁷B. S. Deaver and W. M. Fairbank, Phys. Rev. Lett. **7**, 43 (1961).
- ¹⁸V. T. Petrashov, V. N. Antonov, P. Delsing, and T. Claeson, JETP Lett. **59**, 551 (1994).
- ¹⁹V. T. Petrashov, V. N. Antonov, P. Delsing, and T. Claeson, Phys. Rev. Lett. 74, 5268 (1995).
- ²⁰W. Belzig, R. Shaikhaidarov, V. V. Petrashov, and Yu. V. Nazarov, Phys. Rev. B **66**, 220505 (2002).
- ²¹ A. V. Galaktionov, A. D. Zaikin, and L. S. Kuzmin, Phys. Rev. B 85, 224523 (2012).
- ²²A. V. Galaktionov, and A. D. Zaikin, Phys. Rev. B **88**, 104513 (2013).
- ²³ V. T. Petrashov, R. Sh. Shaikhaidarov, I. A. Sosnin, P. Delsing, T. Claeson, and A. Volkov, Phys. Rev. B 58, 15088 (1998).
- ²⁴E. Strambini, F. S. Bergeret, and F. Giazotto, Appl. Phys. Lett. **105**, 082601 (2014).
- ²⁵F. Giazotto, T. T. Heikkilä, A. Luukanen, A. M. Savin, J. P. Pekola, Rev. Mod. Phys. **78**, 217 (2006).
- ²⁶FastHenry version 3.0wr, by Stephen R. Whiteley, available at http://wrcad.com.
- ²⁷K. D. Usadel, Phys. Rev. Lett. **25**, 507 (1970).
- ²⁸J. C. Hammer, J. C. Cuevas, F. S. Bergeret, and W. Belzig Phys. Rev. B 76, 064514 (2007).
- ²⁹H. Rabani, F. Taddei, F. Giazotto, and R. Fazio, J. Appl. Phys. **105**, 093904 (2009)
- ³⁰N. Schopohl, and K. Maki, Phys. Rev. B **52**, 490 (1995).
- ³¹M. Eschrig, Phys. Rev. B **61**, 9061 (2000).
- ³²V. Yu Nazarov, Superlattices Microstruct. **25**, 121 (1999).
- ³³J. Kopu, M. Eschrig, J. C. Cuevas, and M. Fogelström, Phys. Rev. B 69, 094501 (2004).
- ³⁴The Nazarov boundaries conditions introduce two additional parameters r and τ which correspond to the transparency and the transmission coefficients of the SN interfaces, respectively. In the convention used here an ideal interface is characterized by r=0 and $\tau=1$. In our case, the calculations shown Figs. 2(c) and (d) are obtained with r=0.33 and $\tau=0.5$.
- ³⁵M. Tinkham, *Introduction to Superconductivity*, 2nd ed. (Dover Publication, New York, 2004).
- ³⁶Here the bandwidth is limited to 60 Hz due to the presence of a 50 nF capacitance in the RF filters. This limit is not intrinsic to the device and can be lifted with cryogenic wiring and filtering optimized for this application.
- ³⁷J. Clarke and A. I. Braginski, *The SQUID Handbook. Vol.1 Fundamentals and Technology of SQUIDs and SQUID Systems*, (WILEY-VCH Publication, Weinheim, 2004).
- ³⁸NF Corporation model LI-75A, $\sqrt{S_V} = 1.5 \,\text{nV}/\sqrt{\text{Hz}}$.
- ³⁹DL Instruments model 1211, $\sqrt{S_I} = 5 \,\text{fA}/\sqrt{\text{Hz}}$.
- $^{40}\Phi_{NS,L^R}\sim \sqrt{hL^R/\pi}<15~{
 m n}\Phi_0/\sqrt{{
 m Hz}}.$
- ⁴¹G. E. W. Bauer, E. Saitoh, and B. J. van Wees, Nat. Mat. **11**, 391 (2012).